Polymer Bulletin (2026) 83:380
https://doi.org/10.1007/s00289-026-06448-9

ORIGINAL PAPER

Green synthesis, development and bioactivity of *Hydrocotyle sibthorpioides*-AgNP-loaded electrospun nanofibers

Feride Demîr[1] · **Ömer Kesmez**[1]

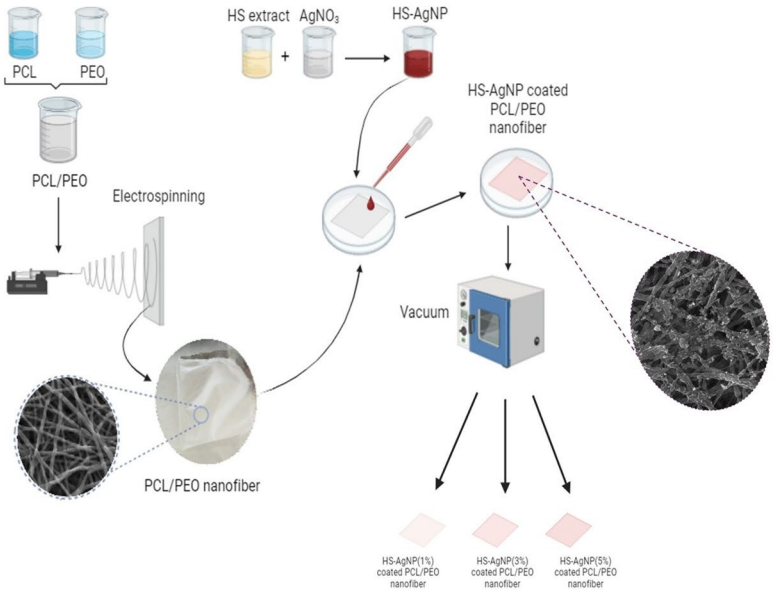
Received: 9 January 2026 / Revised: 13 April 2026 / Accepted: 20 April 2026 /
Published online: 28 April 2026
© The Author(s) 2026

Abstract

The development of advanced wound dressings is crucial for accelerating the healing process and preventing infections. In this study, silver nanoparticles (HS-AgNPs) were synthesized using *Hydrocotyle sibthorpioides* (HS) extracted through an eco-friendly green method and incorporated into polycaprolactone/polyethylene oxide (PCL/PEO) nanofibers produced by electrospinning. The HS-AgNPs were characterized by UV-Vis spectroscopy, SEM, DLS, zeta potential, and FTIR analyses, which confirmed their spherical morphology, nanoscale size distribution (20–80 nm), and high colloidal stability. Phytochemical screening of the HS extract revealed bioactive compounds such as flavonoids, tannins, and alkaloids, which functioned as reducing and stabilizing agents during nanoparticle formation. PCL/PEO nanofibers coated with different AgNP concentrations (1%, 3%, and 5%) were successfully fabricated, showing uniform nanoparticle coated. Structural, mechanical, and thermal analyses demonstrated that AgNP incorporation improved the fibers' stability and performance. Antibacterial activity assays against *Escherichia coli (E.coli)* and *Staphylococcus aureus (S.aureus)* revealed a concentration-dependent effect, with 5% AgNP-coated nanofibers achieving more than 99.99% bacterial reduction. Cytocompatibility studies with L929 fibroblast cells confirmed that all formulations maintained high cell viability, with no statistically significant cytotoxic effects observed. Overall, the HS-AgNP coated PCL/PEO nanofibers exhibited excellent antibacterial efficacy, enhanced stability, and reliable biocompatibility. These findings highlight the potential of HS-based green-synthesized AgNPs as a sustainable and effective approach for the development of multifunctional wound dressing materials in biomedical applications.

Extended author information available on the last page of the article

Graphical abstract



Keywords Green synthesis · Silver nanoparticles · *Hydrocotyle sibthorpioides* · Electrospinning · Hybrid nanofibers · Wound dressing

Introduction

The skin is the body's primary external defense system. When damaged by trauma, surgery, ulcers, or infection, this protective function is disrupted, and scarring can occur [1]. Wound dressings are vital in directly managing the healing process. The correct dressing is selected by evaluating criteria such as wound type, exudate amount, and infection status, and provides the ideal microenvironment necessary for healing [2]. By protecting against infection, accelerating healing, and protecting from UV radiation, wound dressings create an optimal environment for skin self-repair [3]. An ideal wound dressing should be biocompatible, flexible, and easy to apply and remove [4]. Traditional dressings only serve as a physical barrier and do not keep the wound moist, which can slow healing and increase the risk of infection [5]. Modern wound dressings deliver active ingredients directly to the wound site, providing a moist environment, preventing infection, and reducing inflammation [6]. Furthermore, their flexible structure allows them to better conform to the wound site and can be easily applied and removed without damaging the tissue [7]. Polymer-based dressings, thanks to their biocompatible and flexible structures, conform perfectly to

the wound bed, preventing fluid accumulation and creating a moist environment to accelerate healing [8]. They actively support healing by releasing active ingredients such as antimicrobial agents and growth factors in a controlled manner. Their lightweight structure and designs prioritize patient comfort, causing minimal tissue irritation [9]. Researchers are currently working to create antimicrobial, functional wound dressing materials that reduce the risk of infection and accelerate the healing process by promoting tissue regeneration [10, 11]. The incorporation of antibacterial and therapeutic agents into the structure of nanofiber wound dressings provides benefits such as exudate absorption, oxygen permeability, and a large surface area, as well as wound healing-supporting properties [12]. Although various techniques have been developed to produce nanofibers, electrospinning is the most beneficial approach due to its low cost, rapid production, and ease of application; its primary disadvantage is its low efficiency [13]. While natural polymers are used in the production of wound dressings by the electrospinning method, synthetic biocompatible polymers are also preferred [14]. PCL is a biocompatible and biodegradable synthetic polyester with FDA approval. Although it is not effective in wound healing on its own due to its lack of biological activity and hydrophobic structure, PCL is widely used in many medical applications, including tissue scaffolds, wound dressings, sutures, and birth control pills [15]. Various methods are available to improve the hydrophilic properties of PCL nanofibers, including plasma treatment [16], UV irradiation [17], chemical oxidation [18], surface coating [19], and incorporation/compositing with hydrophilic polymers (such as poly(vinyl alcohol) (PVA)) or poly(oxyethylene) (PEO)) [20]. PEO is an FDA-approved synthetic polymer that dissolves in both water and organic solvents and is biodegradable, biocompatible, and non-toxic [21]. Its incorporation into PCL enhances cell adhesion and biocompatibility by increasing the water contact angle and surface energy [22]. Today, modern-generation dressings are specifically designed to deliver active pharmaceutical ingredients directly to the wound site [23]. *Hydrocotyle sibthorpioides* (HS) (family *Apiaceae*) is a perennial plant traditionally used by people in India and China for the treatment of various diseases [24]. HS supports mental functions [25], is an antipyretic [26], reduces edema [27], and relieves pain [28]. Thanks to its effects, it is a frequently used plant in traditional medicine. It also helps detoxify the body [29]. It is known to be useful in the treatment of various diseases such as immune system problems [30], hepatitis [31], rheumatic disorders [32], jaundice [33], and dysentery [34]. Studies show that this plant can also effectively prevent tumor formation [35]. On the other hand, pharmacological studies have shown that the plant exhibits anti-diuretic activity and is effective against skin tumors in external applications [36]. Hazarika et al. reported that HS extracts are safe at a dose of 2000 mg/kg according to OECD 425, show no significant toxicity, and provide potential safety in the treatment of inflammatory diseases [37]. Because traditional chemical synthesis methods involve toxic substances that are unsuitable for biomedical use, researchers are turning to green chemistry approaches that offer safer, biocompatible, and environmentally friendly solutions for nanoparticle production to overcome these limitations. Green synthesis approaches stand out in nanoparticle production due to their cost-effective, environmentally friendly, and biologically safe characteristics, while the use of plant extracts makes the process faster, more sustainable, and more suitable for large-scale production [38]. There are several routes to

produce silver nanoparticles (AgNPs), including chemical reduction [39], radiolysis [40], electrochemical synthesis [41], and bacterial synthesis [42]. Currently, there is significant interest in AgNPs produced using green synthesis methods using plants [43]. Synthesis using plant extracts is a widely preferred biological method for AgNP production due to its ease of application, rapid results, low cost, non-toxicity and non-pathogenicity, biocompatibility, and broad potential for use in many biomedical fields [44]. Organic compounds present in plant extracts reduce silver ions (Ag^{+}) to form elemental silver (Ag^{0}); they also influence the size, stability, and surface properties of nanoparticles, affecting biocompatibility and solubility [45]. Garg et al. synthesized AgNPs using ethyl acetate extract of HS with an environmentally friendly approach and showed that these nanoparticles showed significant antibacterial activity against multidrug-resistant *Staphylococcus aureus (S. aureus)*, *Pseudomonas aeruginosa (P. aeruginosa)*, and *Klebsiella pneumonia (K. pneumonia)* strains [46]. Considering the various limitations of traditional wound dressings and the increasing need for multifunctional biomaterials, the use of silver nanoparticles obtained through green synthesis methods stands out as a remarkable solution. HS, a medicinal plant rich in bioactive components, offers a natural resource capable of performing both reduction and stabilization tasks in nanoparticle production. Combining HS-AgNPs synthesized from HS with polymeric nanofiber structures not only provides strong antibacterial properties but also improves the physicochemical properties of wound dressings. In this study, silver nanoparticles were synthesized using HS plant extract, and then these nanoparticles were integrated into PCL/PEO-based nanofiber wound dressings to enhance antibacterial efficacy. The unique aspect of this study is the first-ever use of nanoparticles obtained from the HS plant in polymeric wound dressings and the detailed investigation of the synergistic effect created by this combination.

Experimental

Materials

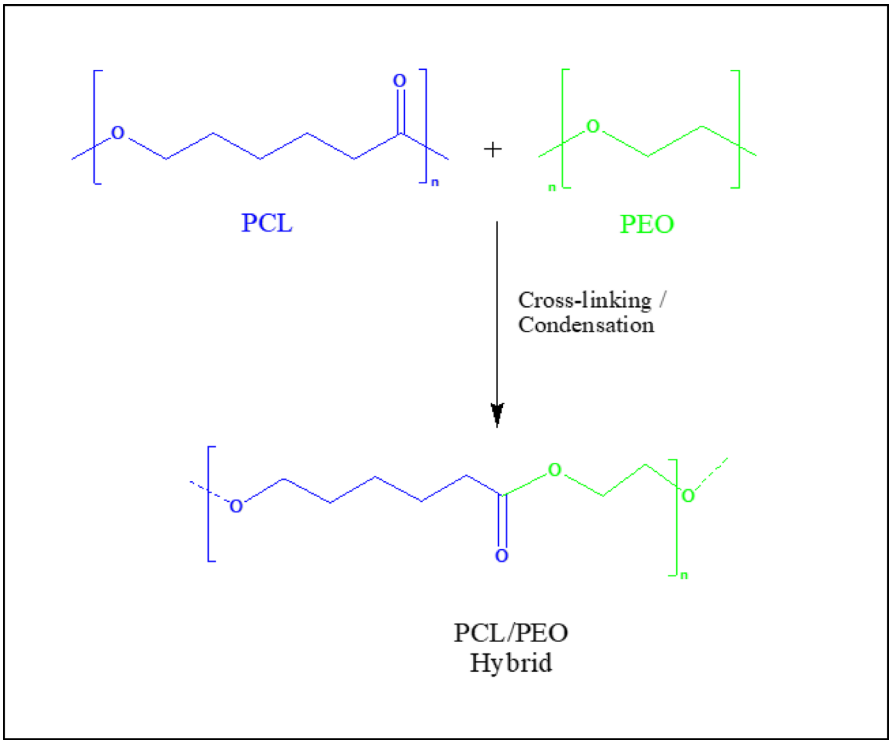
PCL (Mn = 80000, No. 440744) and PEO (Mv = 300000, No. 182001) for hybrid nanofibers were purchased from Sigma-Aldrich (Germany). HS plant was supplied wet and fresh from AkvaRED (Türkiye). $AgNO_3$ (cryst. extra pure), ethanol (≥99.9% purity), and chloroform (99.0% purity) were purchased from Merck. For the antimicrobial activity tests, *S. aureus* (ATCC 6538) and *E. coli* (ATCC 10536) were used. All the microbial culture media used in this study were purchased from Merck. For cell culture studies, L-929 mouse fibroblast cells (ATCC® CCL-1™) were obtained from the American Type Culture Collection. Fetal bovine serum (FBS) and Penicillin-Streptomycin were provided by Sigma-Aldrich (Germany). To evaluate cytotoxicity, 3-[4,5-dimethylthiazol-2-yl]-2,5-diphenyltetrazolium bromide (MTT) reagent and dimethyl sulfoxide (DMSO) were purchased from Sigma-Aldrich (Germany).

Green synthesis of AgNPs by HS (HS-AgNP)

Fresh HS was washed with distilled water immediately after procurement and dried in the shade at room temperature. The ethanol-water (10:90, v/v) solvent system was selected to enhance the extraction efficiency of polar phytochemicals such as flavonoids, phenolic acids, and tannins, which are known to play a critical role in the reduction and stabilization of metal nanoparticles. Approximately 10 g of plant powder was extracted via Soxhlet extraction using 250 mL of ethanol-water (10:90, v/v) at 85 ± 3 °C for 6 h, corresponding to approximately 20–25 extraction cycles. For AgNP synthesis, an aqueous solution of plant extract at a concentration of 1% (w/v) was prepared. The pH of the reaction medium was measured at 5.5 and maintained without any adjustment. Reaction conditions were optimized through preliminary experiments to ensure controlled nucleation and growth of nanoparticles, prevent excessive aggregation, and obtain a homogeneous size distribution. According to the optimum method, the HS extract was mixed with a 1 mM $AgNO_3$ solution in a 7:3 (w/w) ratio and stirred on a magnetic stirrer at 28 ± 1 °C and 850 rpm for 6 h. The reaction was conducted in the dark to prevent photo-induced reduction of Ag^+ ions, ensuring that the nanoparticle formation was primarily governed by phytochemical-mediated reduction [47]. The extract solution, which was initially yellow in color, turned transparent when $AgNO_3$ was added and then turned reddish brown during the synthesis process. The resulting mixture continued to be stirred at room temperature and in the dark for 24 h until this color change became stable [48]. The formation of HS-AgNPs was monitored qualitatively by color change and simultaneously by UV-vis spectrophotometer for 3 h and was characterized quantitatively by DLS and zeta meters. The synthesized HS-AgNPs were filtered through a 0.45 µm filter (Schleicher & Schuell SS FP 030/2 Einmal-Filternalter) and stored at + 4 °C.

Electrospinning process of the hybrid nanofibers

The PCL/PEO ratio was determined based on preliminary optimization studies evaluating different polymer ratios and corresponding solvent compositions. For the electrospinning process of hybrid nanofibers, PCL (10%, w/v) and PEO (2%, w/v) solutions were dissolved in a chloroform/methanol (1:1, w/v) mixture and stirred overnight. Different electrospinning parameters such as flow rate, applied voltage, and processing time were adjusted for each formulation. The 1:1 ratio ensured stable jet formation and uniform nanofiber morphology; therefore, it was chosen for subsequent experiments. Determined amounts of PCL and PEO solutions were mixed to prepare the PCL/PEO mixture (1:1, w/w) and stirred overnight before the electrospinning process (Scheme 1). An electrospinning system (Inovenso-NE300) consisting of a high-voltage source, an aluminum rotary cylinder collector, and a syringe pump was used for the synthesis of PCL, PEO, and PCL/PEO nanofibers. A 10 mL plastic syringe with a stainless-steel needle was used for the PEO solution, while 10 mL glass syringes were preferred for PCL and PCL/PEO solutions. The syringes were individually placed in a system with a single syringe pump and positioned at a 90° angle to the cylinder collector. Flow rates were optimized as 5.5 mL/hr, 3.0 mL/hr, and 3.5 mL/hr for PCL, PEO, and PCL/PEO hybrid nanofibers, respectively. The



Scheme 1 PCL/PEO hybrid formation because of PCL and PEO reaction

applied voltage was fixed at 25.5 kV for PCL and 25 kV for PEO and PCL/PEO, while the rotary drum collector speed was maintained at 300 rpm. The electrospinning process lasted approximately 4 h, and all experiments were performed under ambient conditions (29 ± 1 °C, 60–70% relative humidity) monitored using a digital thermo-hygrometer (UNI-T A12T) [49].

Coating of PCL/PEO nanofibers with HS-AgNPs

After the electrospinning process was completed, a coating method was applied to the resulting PCL/PEO hybrid nanofiber wound dressings using a colloidal AgNP-containing HS-AgNP solution to impart antibacterial properties. PCL/PEO nanofiber wound dressings were cut into 5 × 5 cm sections, and the average weight of each sample was determined to be 0.025 ± 0.002 g. The Ag content of the HS-AgNP solution was determined gravimetrically, and it was calculated that 100 g of HS-AgNP solution contained 9.72×10^{-3} g of Ag. Accordingly, the required solution amounts for coating the nanofibers to contain 1%, 3%, and 5% AgNP by weight were calculated as 2.57 g, 7.71 g, and 12.86 g, respectively. The cut nanofiber samples were coated with the determined amounts of HS-AgNP solutions under vacuum at 40 °C. This process ensured effective penetration of the solution into the nanofiber matrix and homogeneous distribution of HS-AgNPs across the surface. The obtained PCL/

PEO nanofiber samples containing 1%, 3%, and 5% AgNP were named HS-AgNP1, HS-AgNP3, and HS-AgNP5, respectively [50, 51].

Characterization of HS-AgNPs

Yield Percentage of HS extract

The percentage yield of the plant extract was calculated as follows:

$$(\text{Yield},\ \%) = \frac{\text{Dry weight of the plant extract (g)}}{\text{Initial weight of the plant extract}} \times\ 100 \tag{1}$$

Phytochemical characterization of *Hydrocotyle sibthorpioides* using HPLC-DAD

Phytochemical characterization of *Hydrocotyle sibthorpioides (HS)* extract was performed using a reverse-phase high-performance liquid chromatography (HPLC) system (Shimadzu Prominence, Japan) equipped with a diode array detector (DAD, SPD-M20A). The system consisted of a CBM-20 A system controller, LC-20AT pump, SIL-20ACHT autosampler, and CTO-10ASVp column oven. Data acquisition and analysis were carried out using LC Solution software. Chromatographic separation was achieved on a Zorbax C18 column (250 × 4.6 mm, 5 µm particle size). The mobile phase consisted of solvent A (3% formic acid in water, v/v) and solvent B (methanol, v/v). The method was adapted from T. Gomes et al. (1999) with slight modifications [52]. Elution was carried out using a gradient program. The initial composition was set at 93% A and 7% B and maintained for 3 min. The gradient was then linearly changed to 72% A and 28% B at 28 min, followed by 67% A and 33% B at 60 min, 58% A and 42% B at 62 min, 50% A and 50% B at 70 min, and 30% A and 70% B at 75 min. Finally, the system was returned to initial conditions (93% A and 7% B) at 90 min for column re-equilibration. Prior to analysis, all samples and mobile phases were filtered through appropriate membrane filters and degassed. The column temperature was maintained constant throughout the analysis.

UV-vis spectroscopy

The optical properties of HS-AgNPs produced via green synthesis were determined using a UV-Vis spectrophotometer (Varian Cary 5000 Bio UV-Vis-Nir Spectrophotometer; Australia). After the addition of 1 mM $AgNO_3$ to 1% HS solution, spectra were recorded in the wavelength range of 300–700 nm at 30 min. intervals for 6 h. The final measurement of the spectra was carried out 24 h following the $AgNO_3$ addition.

Dynamic light scattering (DLS) and zeta potential

To study the size distribution and stability of HS-AgNPs, their average hydrodynamic diameter and zeta potential values were determined by dynamic light scat-

tering (DLS) analysis using a Zeta-Sizer device (Nano ZS, Malvern Instruments, Malvern, UK).

Scanning electron microscopy (SEM)

Morphological analysis of HS-AgNPs was performed by the Middle East Technical University (METU)-Merlab using SEM (QUANTA 400 F Field Emission, Turkey).

Fourier-transform infrared (FT-IR) analysis

IR spectra of HS extracts and synthesized HS-AgNPs were obtained by the attenuated total reflectance (ATR) method in the mid-IR region between 400 and 4000 cm^{-1} using an FTIR spectrometer (Shimadzu, QATR-S, Japan). This characterization was used to investigate the structural changes induced by the addition of HS extract.

Phytochemical test

According to the methods reported in the literature, qualitative phytochemical analysis was performed to evaluate the presence of different classes of phytochemical compounds in the HS extract [53].

Characterization of HS-AgNP coated PCL/PEO hybrid nanofiber wound dressings

FT-IR analysis

Functional group analysis of the hybrid nanofibers was performed using FTIR spectroscopy (Shimadzu, QATR-S, Japan). Each sample was examined in the mid-infrared (MIR) region in the wavelength range of 400–4000 cm using attenuated total reflection (ATR) coupling.

SEM analysis

To determine the HS-AgNPs on the surface of the electrospun fibers, the morphological characteristics of the nanofibers were analyzed by METU using SEM (QUANTA 400 F Field Emission, Turkey). Dimensional analysis of nanofibers and HS-AgNPs was performed using Image J program.

Thermogravimetric (TGA) analysis

Thermogravimetric analysis (TGA) was used to study the heat properties of the hybrid nanofiber wound dressings using a TGA analyzer (TGA, STA6000/8000, PerkinElmer Instruments, USA). A TGA thermogram was created by heating the samples from room temperature to 500 °C at a rate of 5 °C/min in an air environment (20.0 ml/min) using a single heating step.

Mechanical analysis

The mechanical properties of hybrid nanofiber wound dressings were evaluated using a tensile tester (Shimadzu AGS-X) in accordance with ASTM D882 standard. Rectangular nanofiber samples, each with dimensions of 10 × 60 mm, were prepared for the test, and the thickness measurements were determined accurately using a digital caliper. Tensile tests were performed by applying a preload of 0.1 N and a constant cross-lattice speed of 10 mm/min. As a result of these tests, mechanical parameters such as tensile strength, elastic modulus, and elongation at break of the samples were determined.

Water absorption capacity analysis (WAC)

The water absorption capacity of the hybrid nanofibers was determined according to ASTM D-570. The water absorption capacity (WAC, %) was calculated as follows:

$$(\mathrm{WAC},\ \%)\ =\ \times 100 \tag{2}$$

where w_0 represents the weight of the nanofibers before immersion in water and w_s represents the weight of the nanofibers 24 h after immersion in water [54].

Water contact angle analysis

Water contact angles were measured using a goniometer (Rame-Hart Inc., Nrl. C.A. Goniometer, France) to assess hydrophobicity/hydrophilicity. A 2 µL ultrapure water droplet was placed on each nanofiber sample, and the angle was determined from captured images using ImageJ software. Reported values are the average of at least five measurements taken at random points per sample.

Antimicrobial activity

The antibacterial activities of HS-AgNP1, HS-AgNP3 and HS-AgNP5 coated PCL/PEO hybrid nanofibers were evaluated using a quantitative colony count reduction procedure according to the modified version of ASTM E2149-10 standard. *E. coli* and *S. aureus* were used as model gram-negative and gram-positive bacteria, respectively. Uncoated nanofibers served as the control group. The surfaces of both control and test samples were inoculated with bacterial suspensions. After 24 h of contact time, bacterial cells were recovered using an appropriate neutralizing solution to quench the antimicrobial activity. Serial dilutions of the recovery solution were plated on nutrient agar, and the number of viable colonies (CFU/ml) was determined after 24 h of incubation at 37 °C. Antibacterial activity was measured by comparing the mean log reduction in viable cells and the corresponding percent reduction with the initial inoculation and the control. All tests were performed in triplicate ($n = 3$), and the results are expressed as mean ± standard deviation (SD).

Cell culture conditions and cytotoxicity assay

For cell culture experiments, L929 (mouse fibroblast) cells were cultured in Dulbecco's Modified Eagle Medium (DMEM) supplemented with 10% fetal bovine serum (FBS, Sigma-Aldrich, Germany), 1% penicillin streptomycin, and 1% L-glutamine (Sigma-Aldrich, Germany). Cells were incubated at 37 °C in a humidified atmosphere containing 5% CO_2. The culture medium was refreshed every two days, and the cells were subculture when they reached 80–90% confluence. For cytotoxicity assessment, cells were seeded into 6-well plates at a density of 1×10^5 cells per well in 2 mL of complete medium. After 24 h of incubation to allow cell adhesion, sterile wound dressing materials containing 1%, 3%, and 5% HS-AgNPs were applied to the corresponding wells. A small, standardized section of each dressing (0.5 cm^2) was carefully placed in direct contact with the cell monolayer using sterile forceps. A control group with no dressing applied was included for comparison. Following the application, the plates were incubated for an additional 24 h under the same conditions. Cell viability was assessed using the MTT (3-[4,5-dimethylthiazol-2-yl]-2,5-diphenyltetrazolium bromide) assay. At the end of the 24-hour exposure period, the wound dressings were carefully removed. Then, 100 µL of MTT solution (0.5 mg/mL in PBS) was added to each well and incubated for 4 h at 37 °C. After incubation, the MTT-containing medium was discarded, and 100 µL of dimethyl sulfoxide (DMSO) was added to dissolve the formazan crystals formed by viable cells. The absorbance of the resulting solution was measured at 570 nm using a microplate reader (Thermo Multiskan SPECTRUM, Waltham, MA). Cell viability was expressed as a percentage relative to the untreated control group.

Statistical analysis

All experiments were performed in triplicate. Results are presented as mean ± standard deviation (SD). Statistical analysis was conducted using one-way analysis of variance (ANOVA) followed by Tukey's post hoc test to evaluate the differences between groups. A p-value of less than 0.05 was considered statistically significant.

Results and discussion

Synthesis, characterization, and morphological analysis of HS-AgNPs

Studies have demonstrated the broad-spectrum antimicrobial and antiviral activity of HS-AgNPs against a wide variety of pathogens, including bacteria, fungi, and viruses. Recently, green synthesis has become a highly attractive alternative for AgNP production due to its low cost, environmental friendliness, and lack of high temperature and pressure requirements. In this context, HS-AgNPs have been successfully synthesized using HS plant extracts. The extraction yield percentages are listed in Table 1. The amount of dried plant was 10 g, and 2.463 g of extract was obtained. The 24.63% yield rate calculated (Eq. 1) in line with these values indicates that the bioactive components of the plant can be extracted at a high rate [46].

Table 1 HS yield percentage of whole plant extract

Plant	Dried plant (g)	Extract (g)	Yield (%)
HS	10	2.463	24.63

HS : *Hydrocotyle sibthorpioides*

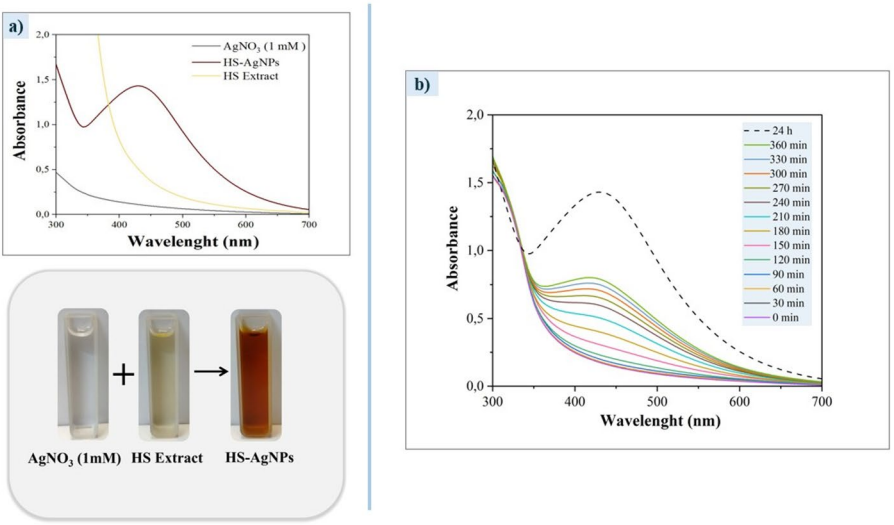


Fig. 1 UV-vis spectra of **(a)** $AgNO_3$ (1 mM), HS extract, and HS-AgNPs with corresponding color changes during nanoparticle formation, **(b)** time-dependent UV-vis spectra showing the gradual formation of HS-AgNPs at different reaction times

The UV-Vis absorption spectrum shown in Fig. 1 shows that HS-AgNPs have a characteristic broad, bell-shaped curve. This spectrum is shaped by the effects of various metabolites in the plant extract added to the solution. These metabolites contributed to the formation of AgNPs by reducing Ag^+ ions to Ag^0, thus broadening the surface plasmon resonance (SPR) and increasing absorption in the spectral range. This is confirmed by the distinct absorption maximum observed at 450 nm. As seen in Fig. 1b, the SPR peak at approximately 450 nm increased over time and reached a maximum at 360 min. AgNP formation can also be observed by the change in solution color; the solution changed from light yellow to reddish brown (Fig. 1a). Peaks observed in the 425–475 nm range indicate AgNP formation. While homogeneous spherical AgNPs normally exhibit an SPR band at 413 nm, the maximum absorption observed at 450 nm in this study can be explained by differences in particle size. Furthermore, the tailing of the spectrum toward longer wavelengths indicates particle size and shape distribution [55]. According to Mie theory, spherical nanoparticles generally exhibit a single SPR band. The narrowing and stabilization of this band observed over time in the UV-Vis spectrum indicates that the particles have formed and their size has stabilized. The presence of a single, distinct SPR peak strongly supports the notion that the synthesized AgNPs are largely spherical and consistent

with Mie theory [56]. These findings are aligned with the previous studies where the synthesized AgNPs displayed [57, 58].

The HS-AgNPs observed in the SEM image (Fig. 2a) are in the size range of approximately 20–80 nm and mostly have a spherical or hemispherical morphology; this is consistent with the naturally occurring FCC (face-centered cubic) crystal structure of silver [59]. In the image, some particles are observed to be in contact with each other or clustered; this shows a relatively wide size distribution, partly due to aggregations formed by van der Waals interactions or surface tension during sample drying. The distinct edge and surface structures of the particles show high crystallinity and directional growth, and it is thought that there may be a crystal orientation dominated by the surface plane. In line with this information, it can be concluded that the silver nanoparticles in the SEM image have a well-defined morphology and crystalline structure and are nano sized [60]. DLS analysis was used to investigate the size distribution of HS-AgNPs synthesized using HS extract. The DLS results presented in Fig. 2b revealed that the average particle size is 37.27 ± 6.4 nm, with most particles distributed between 20 and 60 nm. Furthermore, the polydispersity index (PDI) values were determined to be in the range of 0.359–0.514, indicating a moderate level of polydispersity in the nanoparticle population. These results show that although the nanoparticles exhibit some size variation, the majority are concentrated around ~ 37 nm. Overall, the findings of this study confirm that HS-AgNPs possess nanoscale dimensions, a well-defined morphology, and a reasonably controlled size

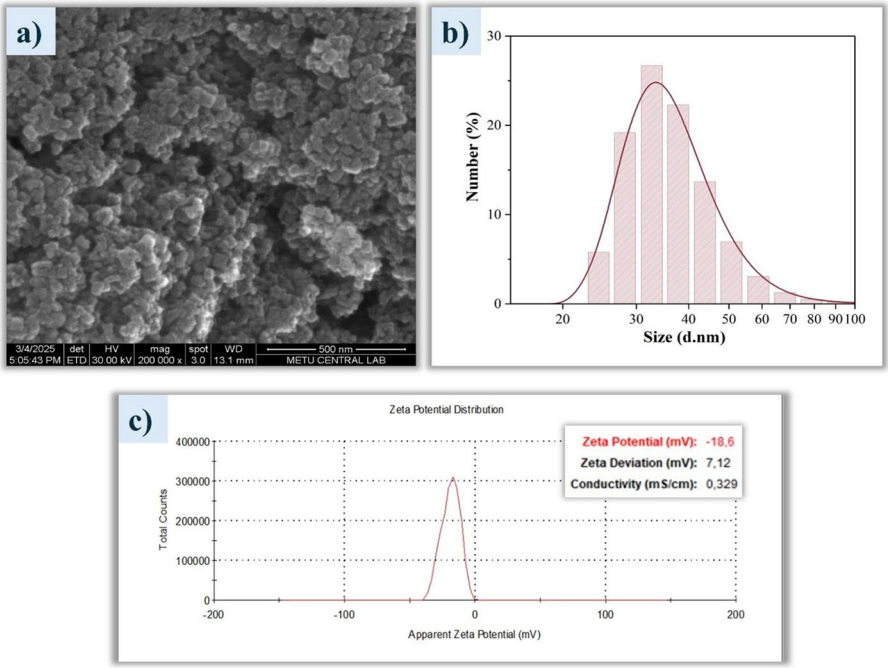


Fig. 2 HS-AgNPs: **(a)** SEM images, **(b)** particle size and **(c)** zeta potential distribution and corresponding stability data

distribution. Moreover, these results contribute to a better understanding of the interactions between AgNPs and microorganisms, highlighting the potential of HS plant extracts as a promising and effective tool for the development of next-generation antibacterial agents [61]. Zeta potential is a measure of surface charge potential used to determine the stability of nanoparticles in aqueous solutions. The zeta potential value of HS-AgNPs was determined as -18.6 ± 3 mV (Fig. 2c). This result indicates that the produced nanoparticles are coated with negatively charged acidic groups in a dispersed environment, leading to electrostatic repulsion between the particles; however, this zeta potential value shows moderate colloidal stability in solutions [62].

The FTIR analysis shown in Fig. 3 was performed to evaluate the functional group interactions between the HS plant extract and HS-AgNPs. Changes in the FTIR spectra support the idea that phenolic hydroxyl, carbonyl, and glycosidic functional groups in the structure of the HS plant play an active role in the reduction of Ag^+ ions and the coating of the AgNP surface. Table 2 presents a detailed analysis of the relevant peaks.

The O-H stretching vibration at 3241 cm^{-1} indicates the interaction of -OH groups that acted as reducing agents in the synthesis of AgNP; the peak shift reflects this interaction. The C-H (aliphatic) stretching band at 2931 cm^{-1} originates from the glycosidic structure and shows a slight decrease after AgNP synthesis and indicates the interaction in the bond structure [63]. The C = O stretching band at 1667/1588 cm^{-1} suggests that aromatic components may have complexed with Ag^+. The C-H bending (phenolic structure) band at 1372 cm^{-1} indicates that aromatic structures in the

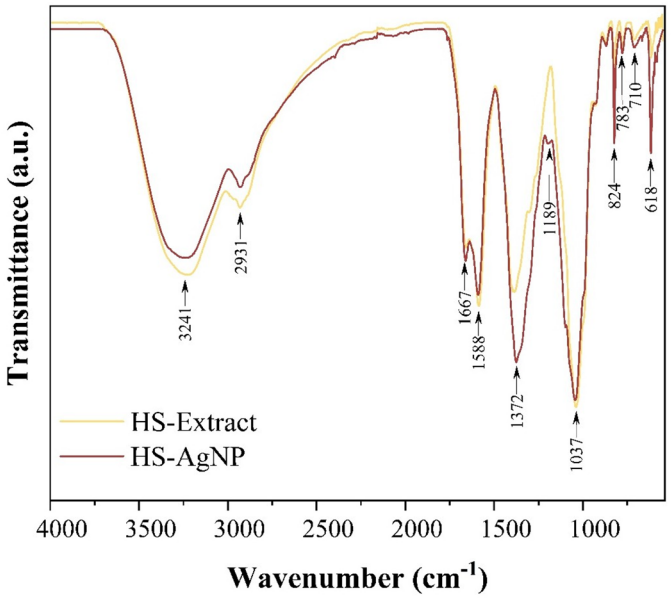


Fig. 3 FTIR Spectra of HS Extract and HS-AgNP

Table 2 FTIR Peak Assignments of HS Extract and HS-AgNPs

Sample	Wavenumber (cm^{-1})	Functional group	Vibration type
HS Extract & HS-AgNP	3241	O-H	Stretching (phenolic/alcoholic)
	2931	C-H (aliphatic)	Stretching
	1667/1588	C = O	Stretching
	1372	C-H (aliphatic)	Bending (phenolic structure)
	1189/1037	C-O	Stretching (alcohol, esters)
	824/783/710	C-H (aliphatic)	Bending
HS-AgNP	618	Ag-O	Coordination vibration

Table 3 Qualitative phytochemical analysis of the leaf extracted from HS

Phytochemical test	Observation result
Triterpenoids	Identified
Flavonoids	Identified
Steroids	Identified
Tannins	Identified
Carbohydrates	Identified
Alkaloids	Identified

active substance may contribute to stabilization. The C-O stretching band (alcohols, esters) at 1189/1037 cm^{-1} is strong evidence that glycosidic bonds and ester groups bind to the AgNP surface, providing stabilization. The C-H (aromatic) bending band at 824/783/710 cm^{-1} shows the presence of aromatic rings and their potential interaction with the nanoparticle surface. The Ag-O coordination vibration at 618 cm^{-1} is a characteristic peak confirming the formation of silver nanoparticles and representing metal-ligand bonds. Spectral shifts and newly formed peaks in the FTIR analysis indicate that functional groups in the plant structure reduce Ag^{+} ions and stabilize the surface of the resulting silver nanoparticles. In particular, the active involvement of -OH, C = O, and C-O groups contribute to understanding the green synthesis mechanism at the molecular level. These results strongly support the idea that *Hydrocotyle sibthorpioides* can be used as a potential bio reducing agent and coating material in sustainable nanotechnology applications [64].

According to the data in Table 3, it was determined that HS extract contained various phytochemical compounds such as triterpenoids, flavonoids, steroids, tannins, carbohydrates, and alkaloids. It is evaluated that compounds with reducing potential, especially flavonoids, tannins, and alkaloids, may play an important role in the process of reducing silver ions to nano-sized silver particles and in the stabilization of these particles [65]. These findings reveal the potential of HS extract to be used as an effective biological reduction and stabilization agent in the production of nanoparticles by green synthesis methods.

The phenolic profile of the HS plant extract was characterized using HPLC-DAD. Identification of individual phenolic compounds was performed by comparing retention times (RT), UV absorption maxima (λmax), and chromatography with available authentic standards. Quantitative analysis was performed using external standard calibration curves, and results were expressed in ppm (mg/L) in the injected solution. Based on a total extract volume of 1.094 g, the absolute content of each compound

Table 4 Phenolic compounds identified and quantified in HS extract by HPLC-DAD

Phytochemical compounds	Retention time (min)	λmax (nm)	Concentration (ppm)	Content in 1.094 g HS (mg)
Gallic acid	6.8	280	17.210	1.721
3,4-Dihydroxy	10.7	280	0.955	0.096
Catechin	15.2	220	22.406	2.241
4-Hydroxy	15.7	280	0.612	0.061
2,5-Dihydroxybenzoic acid	17.2	320	3.549	0.355
Chlorogenic acid	18.2	320	0.041	0.004
Vanillic acid	19.2	320	14.703	1.470
Epicatechin	21.3	260	5.219	0.522
Caffeic acid	22.7	280	125.891	12.589
p-Coumaric acid	26.1	320	2.654	0.265
Ferulic acid	30.1	320	10.539	1.054
Rutin	45.6	360	1.675	0.168
Ellagic acid	47.7	240	64.791	6.479
Quercetin	70.4	360	26.920	2.692
Cinnamic acid	71.1	280	7.468	0.747
Narindin	-	-	4.841	0.484

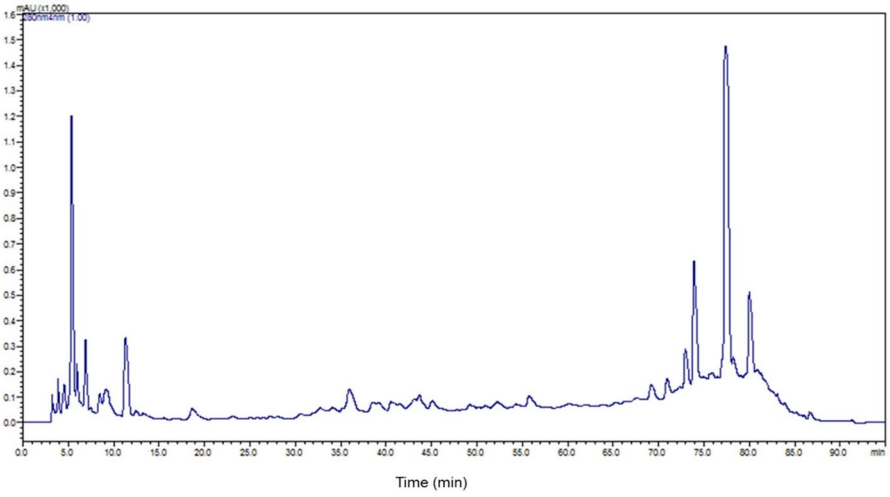


Fig. 4 HPLC-DAD chromatogram of HS extract at 280 nm with retention times (min) shown above the peaks

was calculated and presented in Table 4. As shown in Table 4, a total of 16 phenolic compounds were identified and quantitatively determined in the HS extract.

Chromatographic separation Fig. 4 revealed well-resolved peaks with retention times ranging from 6.8 min to 71.1 min. The most abundant compound was caffeic acid (125,891 ppm in solution; 12,589 mg in 1,094 g of extract), followed by ellagic acid (64,791 ppm; 6,479 mg), quercetin (26,920 ppm; 2,692 mg), and catechin (22,406 ppm; 2,241 mg). Significant amounts of gallic acid (17,210 ppm; 1,721 mg),

vanillic acid (14,703 ppm; 1,470 mg), and ferulic acid (10,539 ppm; 1,054 mg) were also detected. The limits of detection (LOD) for the analyzed compounds ranged from 0.01 to 0.75 ppm, demonstrating the high sensitivity of the developed HPLC-DAD method. The lowest LOD values were obtained for gallic acid, caffeic acid, p-coumaric acid, cinnamic acid, and ferulic acid (0.01 ppm each), while 2,5-dihydroxybenzoic acid showed the highest LOD value (0.75 ppm). Among the identified compounds, flavonoids (catechin, epicatechin, quercetin, rutin, narindin) and phenolic acids (caffeic, ellagic, gallic, vanillic, ferulic, p-coumaric, cinnamic, chlorogenic acids) constituted the main fractions. The presence of these bioactive compounds is particularly noteworthy, as their antioxidants, anti-inflammatory, and antimicrobial properties are well-known [66]. Caffeic acid was the dominant compound, accounting for approximately 40% of the total measured phenolic content. This finding is consistent with previous reports showing that caffeic acid derivatives are the major phenolic components in *Hydrocotyle* species and contribute significantly to their biological activity. Furthermore, high levels of catechin (2,241 mg) and epicatechin (0,522 mg) are in good agreement with the literature in which these flavonoids are identified as significant contributors to the free radical scavenging capacity of HS extracts [67]. The presence of ellagic acid (6,479 mg), a dimeric derivative of gallic acid, is of particular interest due to its well-documented wound healing properties. Ellagic acid has been shown to promote collagen synthesis, inhibit matrix metalloproteinases (MMPs), and reduce oxidative stress in dermal tissues. Similarly, quercetin (2,692 mg) and rutin (0,168 mg) are known to enhance capillary integrity and accelerate the proliferative phase of wound healing [68]. In conclusion, HPLC-DAD analysis of the HS plant extract (1.094 g) revealed a rich phenolic profile dominated by caffeic acid (12.589 mg), ellagic acid (6.479 mg), quercetin (2.692 mg), and catechin (2.241 mg). The total measured phenolic content was approximately 31.48 mg, representing 2.88% of the dry extract weight. These findings are consistent with previous reports identifying catechin, epicatechin, quercetin, and chlorogenic acid as the major antioxidants in HS; however, this study also highlights the importance of caffeic and ellagic acids. The phenolic composition directly supports the multifunctional wound healing properties of HS-AgNP-coated PCL/PEO nanofibers, including antioxidant defense, anti-inflammatory activity, antimicrobial synergy, and promotion of tissue regeneration. These results validate the traditional use of HS in wound management and provide a chemical basis for its application in modern biomedical dressings.

The phytochemical composition of the HS plant extract is thought to play a crucial role in controlling the size and stability of the synthesized HS-AgNPs. HPLC-DAD analysis revealed a high proportion of phenolic compounds, such as caffeic acid, ellagic acid, quercetin, and catechin, known for their strong reducing and coating capabilities. The presence of abundant hydroxyl and carbonyl functional groups in these compounds facilitated the rapid reduction of Ag^{+} ions, leading to controlled nucleation and the formation of relatively small nanoparticles (20–80 nm). In addition, these phytochemicals adsorbed onto the nanoparticle surface, forming a stabilization layer that limits aggregation; this is consistent with the observed moderate zeta potential (-18.6 mV) and size distribution. Therefore, the combined HPLC, FTIR, and DLS results demonstrate a direct structure-function relationship between the

phytochemical profile of the extract and the physicochemical properties of the resulting nanoparticles.

Morphological characterization of PCL/PEO hybrid nanofibers coated with HS-AgNP

The chemical compositions of PCL, PEO, optimized PCL/PEO, and HS-AgNP coated PCL/PEO nanofibers were analyzed using FTIR (Fig. 5). When the spectrum of PCL nanofiber is examined, it is seen that the frequencies around 2939 cm^{-1} and 2860 cm^{-1} generally belong to aliphatic C-H stretching vibrations originating from methylene groups in the polymer chain of PCL. The sharp peak around 1718 cm^{-1} is a characteristic feature of PCL corresponding to the stretching vibration of the ester carbonyl group (C = O). The complex peaks in the rest of the spectrum (below 1500 cm^{-1}) show the stretching vibrations of C-O-C bonds and bending vibrations of C-H bonds of PCL [69]. The peak around 2883 cm^{-1} in the spectrum of PEO nanofibers is a characteristic feature of PEO, belonging to the C-H stretching vibrations of ether groups (-CH_2-O-). Peak around 1464 cm^{-1}: This peak corresponds to -CH_2 bending vibrations. The peak around 1341 cm^{-1} represents C-O-C bending vibrations. The peaks in the rest of the spectrum (1200 –1000 cm^{-1} range) are associated with the ether bonds of PEO, such as C-O-C stretching vibrations [70]. The nanofibers of the PCL/PEO combination showed characteristic peaks of both structures. There are C-H stretching peaks around 2939 cm^{-1} and 2860 cm^{-1} (from PCL) and 2883 cm^{-1} (from PEO). The ester carbonyl (C = O) peak around 1718 cm^{-1} (from PCL) was still prom-

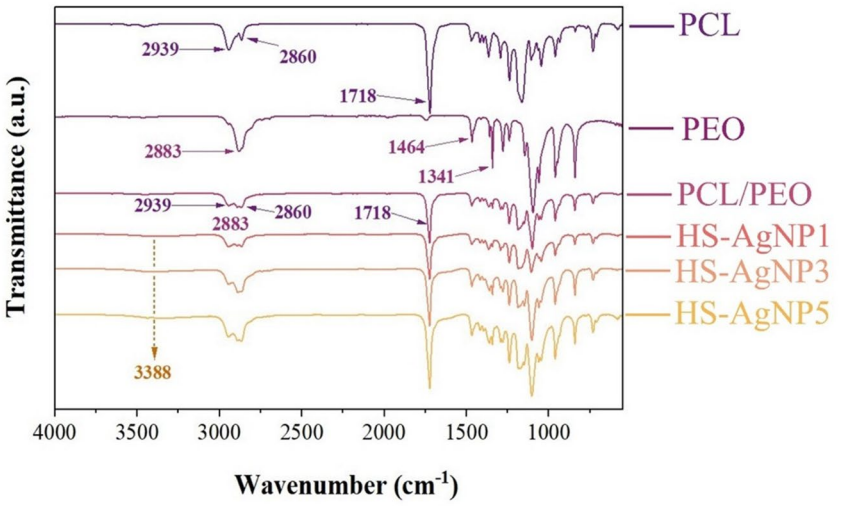


Fig. 5 FTIR Spectra of PCL, PEO, PCL/PEO, and HS-AgNP coated PCL/PEO Nanofibers

inent. Peaks around 1464 cm^{-1} and 1341 cm^{-1}, which are specific to PEO, were also observed; however, their intensities were lower than those in the PEO-only spectrum, indicating a lower PEO ratio in the mixture This spectrum demonstrates the physical mixing of PCL and PEO and confirms the presence of functional groups in both polymers. When the spectra of HS-AgNP1, HS-AgNP3, and HS-AgNP5 nanofibers were examined, it was observed that they were essentially like the spectrum of the PCL/PEO blend. However, the broad and low-intensity hydroxyl (O-H) peak around 3388 cm^{-1} (marked with a dashed arrow) corresponds to the stretching vibration of the O-H groups. This change is due to the presence of the HS stabilizer and -OH groups in the molecular structure of the active ingredient, asiaticoside. An increase in the intensity of this peak was observed as the amount of HS-AgNP increased [71].

Figure 6 shows the SEM images and diameter distributions of different layers of PEO, PCL, PCL/PEO, and HS-AgNP5 nanofibers produced using the single-nozzle electrospinning method under the same environmental conditions. The nanofibers produced with 10% PCL solution had a smooth, parallel structure without bead structures (Fig. 6a). The average fiber diameter was determined to be 287.13 ± 69.0 nm. PEO has a lower viscosity, allowing the formation of thinner fibers. The smooth, bead-free, and smooth nanofibers produced with 2% PEO had an average fiber diameter of 171.08 ± 48.5 nm (Fig. 6b). The fiber diameters were smaller and narrowly distributed. The average fiber diameter of the nanofibers obtained with the PCL/PEO combination was measured as 266.92 ± 82.3 nm (Fig. 6c). Although the fiber structure appeared somewhat more complex and irregular, the fibers were well interconnected. The combined use of PCL and PEO resulted in a wide distribution and variety of fiber diameters. Such combinations are used to optimize mechanical and biological properties. The average diameter of the HS-AgNP5 nanofibers was measured as 336.59 ± 78.7 nm (Fig. 6d). The addition of HS-AgNPs resulted in a significant increase in the diameter of the nanofibers. Analysis of SEM images clearly reveals that HS-AgNPs both adsorbed individually onto the fiber surfaces and concentrated in certain regions to form clusters (agglomerates). This indicates that the nanoparticles provided sufficient contact time and effective surface interaction with the fiber structure during the coating process. This observed structure proves that the HS-AgNPs successfully integrated into the nanofiber matrix to impart antibacterial functionality. While the PCL/PEO nanofibers shown in Fig. 6c exhibit a smooth, fine, homogeneous surface structure, the HS-AgNP5-added samples in Fig. 6d show significant surface roughness, nanoparticle accumulation, and an increase in fiber diameter. This contrast demonstrates that HS-AgNPs, physically bonded to the fiber surface via coating, directly alter the fiber morphology. Adsorption of nanoparticles on the surface is the primary factor increasing fiber roughness. Quantitatively, the average fiber diameter increased from 266.92 nm in PCL/PEO nanofibers to 336.59 nm in HS-AgNP5 nanofibers. The increase in the average fiber diameter of the nanofibers was attributed to the penetration of the HS-AgNP solution used in the coating process into the fiber structure, creating a swelling effect, and the adhesion of HS-AgNPs to the fiber surface [72, 73].

The hydrophilic properties of wound dressings, including water contact angle and absorption, are presented in Fig. 7. Increased hydrophilicity promotes wound healing by improving biocompatibility and cellular activity, while also reducing the risk of infection through optimal moisture retention and ensuring material effectiveness. The

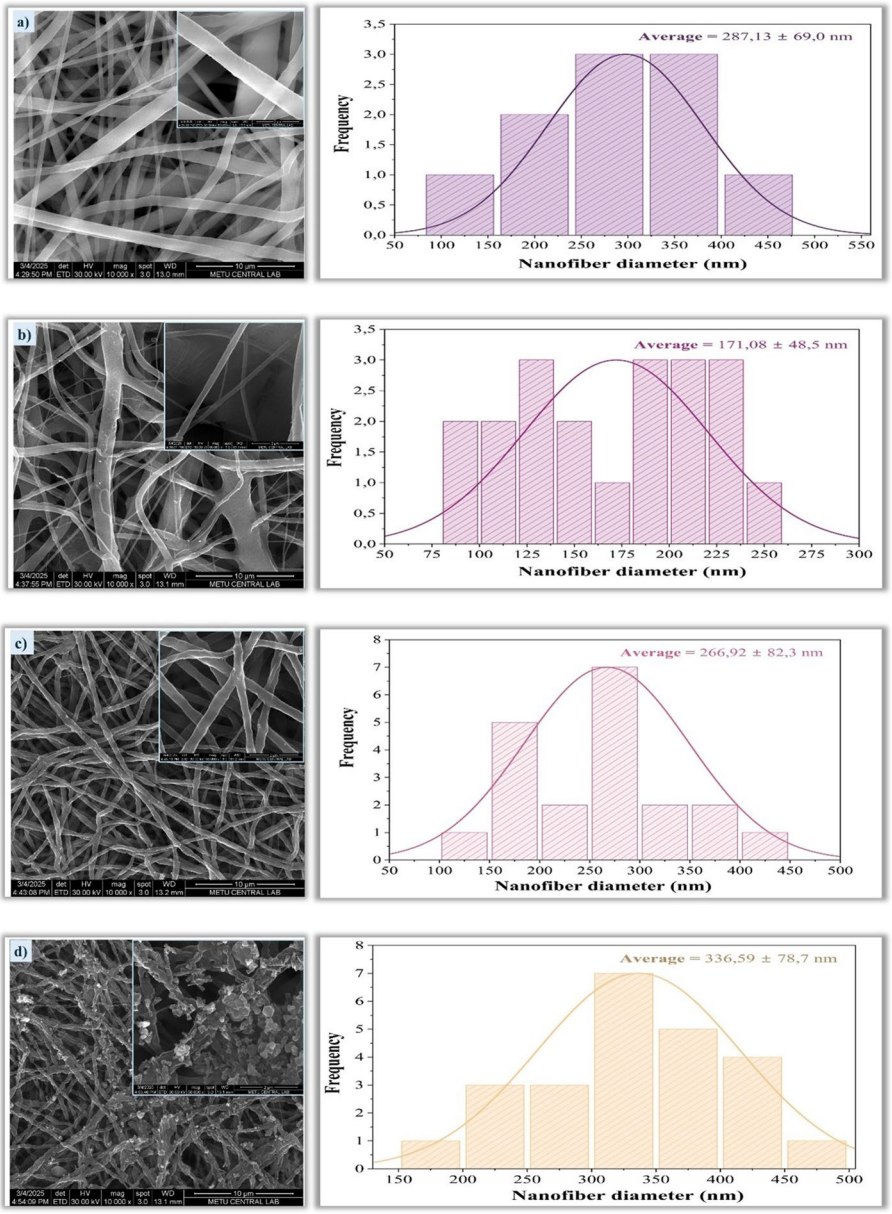


Fig. 6 SEM images and diameter distribution of nanofibers from **(a)** PCL, **(b)** PEO, **(c)** PCL/PEO and **(d)** HS-AgNP5

measured average contact angles of the synthesized PCL (Fig. 7a), PEO (Fig. 7b), PCL/PEO (Fig. 7c), and HS-AgNP5 nanofibers (Fig. 7d) were found to be 141.3 ± 2.3°, 28.8° ± 2.1°, 55.24 ± 3.1°, and 41.4 ± 1.7°, respectively. PCL/PEO nanofibers gained significant wettability and adsorbed water droplets compared to pure PCL due

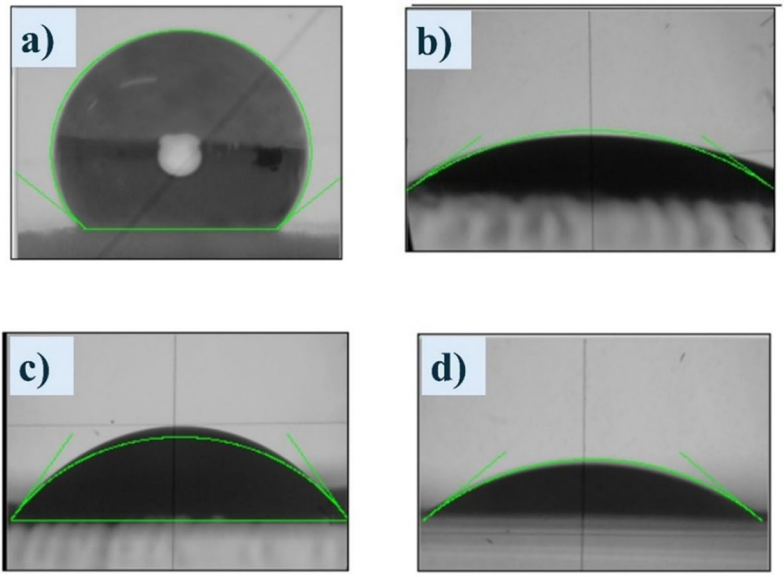


Fig. 7 Water contact angles of nanofibers of **(a)** PCL, **(b)** PEO, **(c)** PCL/PEO, and **(d)** HS-AgNP5

to the hydrophilic PEO on their surfaces. Moreover, the contact angle in HS-AgNP5 nanofibers decreased further compared to PCL/PEO nanofibers, and their wettability increased. This change can be explained by the fact that hydrophilic nanoparticles increase the hydrophilicity of the nanofiber surface, as well as change the surface free energy, surface roughness, and heterogeneity. The results clearly show that HS-AgNP5 nanofibers exhibit hydrophilic properties [74].

Water absorption capacities of hybrid nanofiber wound dressings were determined according to ASTM-D570 standard [75]. Cross-linked wound dressings maintained their nanofiber structure and remained stable against water when immersed in 20 ml of DI water at 25 °C for 24 h. The absorption capacities of HS-AgNP5 and pure PEO/PCL nanofibers were calculated as 186% and 92%, respectively (Eq. 2). In the produced hybrid nanofiber structures, water penetrates the dressing through the channels formed by the PEO nanofibers; since PCL is insoluble in water, it acts as a barrier, allowing water retention within the dressing. According to the obtained results, HS-AgNP-coated PCL/PEO nanofibers showed better absorption capacity than pure electrospun PCL/PEO. As a result, the obtained nanofiber wound dressings have a high-water retention capacity and provide a suitable environment for wound healing by absorbing excess exudate from the wound area [76].

To determine the mechanical properties of the obtained samples, tensile strength and elongation at break tests were performed according to ASTM-D882 standards [77]. To evaluate the mechanical properties of the obtained samples, tensile strength and elongation at break tests were conducted in accordance with ASTM D882 stan-

dards. The measured tensile strengths of PCL, PCL/PEO, HS-AgNP1, HS-AgNP3, and HS-AgNP5 samples were 5.20, 3.64, 3.58, 3.41, and 3.22 MPa, respectively. Correspondingly, the elongation at break values were determined as 212.03%, 91.89%, 89.47%, 84.23%, and 79.56%. As illustrated in Fig. 8, the incorporation of PEO into the PCL matrix led to a significant reduction in both tensile strength and elongation at break, indicating a decline in ductility and overall mechanical performance. This behavior can be attributed to the limited compatibility between the polymer phases and the disruption of the highly ordered crystalline structure of PCL by PEO. Furthermore, the progressive decrease in mechanical properties with increasing concentrations of HS-AgNPs can be explained by their tendency to create discontinuities and stress concentration points within the polymer matrix, thereby weakening its load-bearing capacity. Consequently, although the material becomes more brittle with increasing silver content, the tensile strength value of 3.22 MPa is still considered adequate to preserve the structural integrity required for wound dressing applications [78].

TGA and DTG curves of PCL/PEO and HS-AgNP5 nanofibers are given in Fig. 9. TGA and DTG analyses of PCL/PEO and HS-AgNP5 samples revealed that the HS-AgNP coating significantly increased the thermal stability of the polymer matrix. The 10%, 30%, and 50% weight loss temperatures were determined as 300, 335, and 370 °C for the pure PCL/PEO sample, and as 325, 355, and 390 °C for the coated sample, respectively. The coating delayed the onset of the main degradation by approximately 25 °C, and the maximum degradation rate reached higher values. In addition, the residual mass fraction after degradation increased from 0.5% for the pure PCL/PEO sample to 20% for HS-AgNP5. This suggests that HS-AgNPs, in addition to their thermally inert structure, slow down the degradation mechanism by restricting the

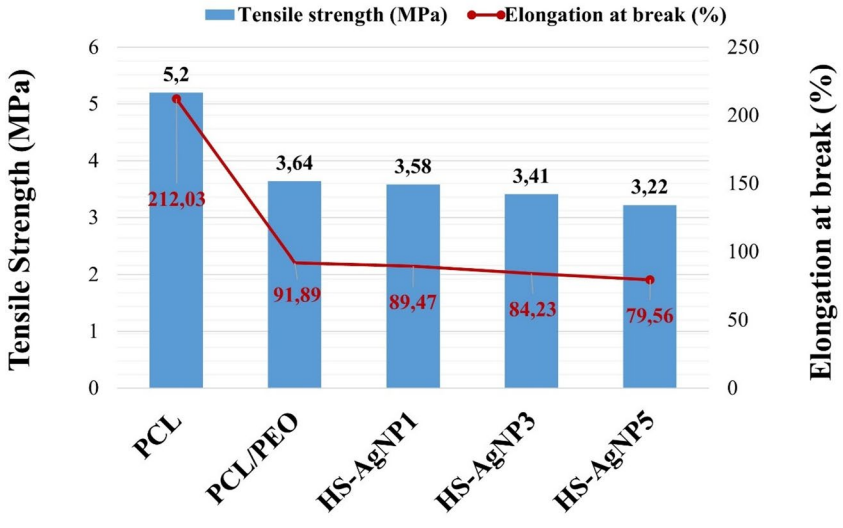


Fig. 8 Comparison of tensile strength and elongation-at-break among the samples

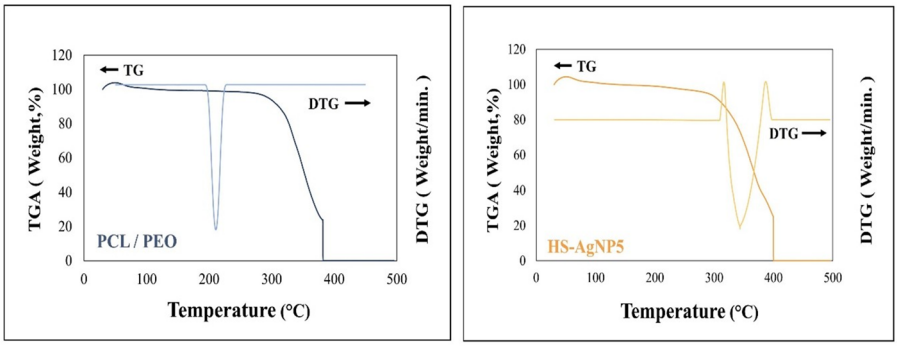


Fig. 9 Thermal degradation behaviors of PCL/PEO and HS-AgNP5 nanofibers

Table 5 Thermal analysis results for the samples

Sample	Weight loss temperature (°C)			Residual (%)
	$T_{10\%}$	$T_{30\%}$	$T_{50\%}$	
PCL/PEO	300	335	370	0.5
HS-AgNP5	325	355	390	20.0

mobility of polymer chains and increasing the high-temperature resistance of the composite [79].

Table 4 summarizes the results obtained from the TGA curves in Fig. 9. The TGA results revealed that the HS-AgNP coating significantly improved the thermal stability of the PCL/PEO matrix. Specifically, the increase in T10% and T50% temperatures indicates that the coating delays the thermal degradation process by restricting the mobility of the polymer chains. Furthermore, the high residual mass percentage confirmed that the HS-AgNPs in the composite were completely inert to degradation.

Antimicrobial activity

In this study, antimicrobial properties were imparted to hybrid materials developed for wound dressing applications by incorporating HS-AgNPs produced via a green synthesis method using *H. sibthorpioides* plant extract. Biopolymer-based nanofiber structures were modified with varying concentrations of Ag^+ to evaluate their efficacy against pathogenic microorganisms. According to a modified version of the ASTM E2149-10 standard, antimicrobial tests were conducted with a 24-hour contact time. The mean $\log_{10}$ CFU/mL and log reduction values (mean ± SD) obtained for *E. coli* and *S. aureus* are presented in Table 5. The antibacterial activity was directly influenced by the Ag^+ concentration within the biocomposite structure [80]. Notably, increasing silver concentrations resulted in a statistically significant increase in antibacterial efficacy ($p < 0.05$), demonstrating a clear dose-dependent response.

Evaluation of the obtained results revealed that the control group, which contained no antibacterial agents, showed no reduction in microbial population; on the contrary, observed population growth clearly demonstrates that these samples lacked bactericidal or bacteriostatic effects. The antibacterial activity of HS-AgNPs is primarily

Table 6 Anti-Bacterial activity against *E. coli* and *S. aureus* of hybrid nanofibers[a]

Sample	*E. coli*			*S. aureus*		
	After 24 h			After 24 h		
	log_{10} CFU/mL	Average reduction, Log_{10}	Average CFU reduction, %	log_{10} CFU/mL	Average reduction, Log_{10}	Average CFU reduction, %
Control	8.376 ± 0.003	-	-	8.326 (±0.002)	-	-
HS-AgNP1	5.305 ± 0.010	0.828 ± 0.010	85.1572 ± 0.2847	5.396 (±0.004)	0.804 ± 0.006	84.2856± 0.1022
HS-AgNP3	2.434 ± 0.011	3.699 ± 0.011	99.9800 ± 0.0005	2.897 (±0.021)	3.303 ± 0.021	99.9501 ± 0.0029
HS-AgNP5	1.307 ± 0.032	4.826 ± 0.032	99.9985 ± 0.0001	1.361 (±0.019)	4.839 ± 0.020	99.9985 ± 0.0001

[a]The mean initial inoculum was 6.133 ± 0.002 and 6.200 ± 0.005 log10 CFU/mL for *E. coli* and *S. aureus*, respectively. Data are presented as mean ± standard deviation (n=3)

attributed to the controlled release of Ag^+ ions from the nanoparticle surface. These ions interact with negatively charged bacterial cell membranes, leading to structural damage and increased membrane permeability [81]. Upon internalization, Ag^+ ions bind to sulfur-containing proteins and DNA, inhibit key enzymes involved in the respiratory chain, and promote the generation of reactive oxygen species (ROS) [82]. Collectively, these mechanisms induce oxidative stress and ultimately result in bacterial cell death. Moreover, the phytochemical corona derived from *Hydrocotyle sibthorpioides* is likely to enhance bio adhesion, thereby strengthening nanoparticle–bacteria interactions and further improving antibacterial efficacy.

This finding confirms that microorganisms in the control samples had complete access to growth resources. In contrast, the presence of 1% silver ions achieved 85.1572% ± 0.2847% and 84.2856% ± 0.1022% reductions in *E. coli* and *S. aureus* populations, respectively. The results demonstrated a statistically significant ($p < 0.05$) concentration-dependent antimicrobial efficacy across all tested groups. Particularly noteworthy was the over 99.9985% ± 0.0001% reduction observed in samples containing 5% silver ions, unequivocally demonstrating the potent antibacterial properties of the synthesized nanofibers. The low standard deviation values across triplicate measurements further confirm the reliability and reproducibility of the antibacterial performance. Considering these findings, the antibacterial effectiveness of the prepared samples shows a direct correlation with silver ion concentration. The utilization of silver ions, especially at higher concentrations, presents an extremely effective strategy for controlling pathogenic microorganisms in living environments, offering promising applications for advanced wound dressing materials [83].

Evaluation of the cytotoxicity

The safe clinical application of wound dressings fundamentally relies on their biocompatibility with host tissues and the absence of any elicited toxic responses. In this study, the in vitro cytotoxicity of the developed PCL/PEO nanofibers coated with green-synthesized HS-AgNPs was evaluated on the L929 murine fibroblast cell line via the MTT assay, in accordance with the International ISO 10993-5:2009 stan-

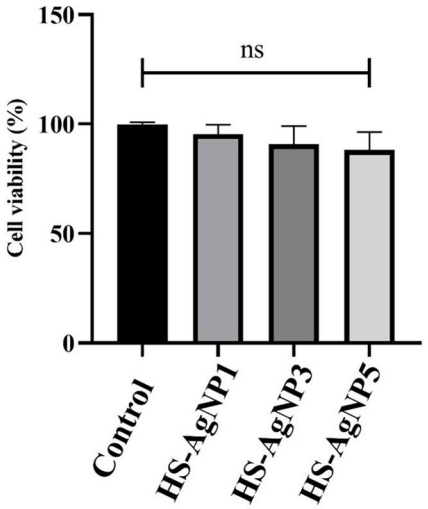


Fig. 10 In vitro cytotoxicity assessment of the PCL/PEO nanofibers modified with green-synthesized HS-AgNPs. The bar chart illustrates the percentage viability of L929 fibroblast cells after 24 h of incubation with the Control, 1%, 2%, and 3% AgNP-loaded nanofiber samples, determined via the MTT assay. Data are presented as mean ± standard deviation (SD). 'ns' indicates that the differences between the AgNP-containing groups and the Control group are not statistically significant ($p > 0.05$) based on one-way ANOVA followed by Tukey's post-hoc test

dard [84]. As illustrated by the cell viability graph in Fig. 10 and the corresponding analysis of variance (ANOVA), the decline in cell viability remained marginal despite increasing silver concentrations. According to the ISO 10993-5:2009 guidelines, material is considered non-cytotoxic if it maintains a cell viability of over 70% relative to the control group [84]. All tested formulations in the present study comfortably exceeded this threshold, confirming the biosafety profile of the hybrid nanofibers. Specifically, following a 24-hour incubation period, the viability of the control group was recorded as 100.00 ± 0.62%. In comparison, the viabilities for the nanofiber samples containing 1%, 2%, and 3% HS-AgNPs were determined to be 95.40 ± 3.44%, 90.87 ± 6.64%, and 88.24 ± 8.28%, respectively. Statistical analysis clearly demonstrated that the incorporation of HS-AgNPs did not induce a statistically significant level of cell death in L929 fibroblasts ($p > 0.05$). Even the difference between the control group and the HS-AgNP5 group, which contained the highest nanoparticle concentration, fell well below the threshold of statistical significance ($p > 0.05$). It is frequently noted in literature that silver nanoparticles can penetrate the cell membrane, interfere with intracellular cycles, and induce dose-dependent cytotoxicity. However, nanoparticles synthesized via green routes are known to exhibit notably higher biocompatibility in mammalian cell lines compared to those produced through traditional chemical reduction methods [83]. A primary reason for this reduced toxicity is that the bioactive molecules derived from the HS plant extract act as capping

agents, wrapping around and stabilizing the AgNP surfaces [85]. Additionally, the entrapment or firm attachment of these particles to a polymer matrix like PCL/PEO modulates the release of Ag^+ ions into the surrounding environment. This controlled release prevents the cells from experiencing acute toxic shock [86]. Our data support this protective polymer-nanoparticle mechanism, given that cellular viability did not drop below the 85% mark at any of the tested concentrations. Ultimately, the findings indicate that the HS-AgNP-modified hybrid PCL/PEO nanofibers do not inhibit the proliferation of L929 fibroblasts. Since the observed cytotoxic effects were statistically insignificant, it is evident that these materials can foster a safe cellular microenvironment for skin regeneration and wound healing while simultaneously delivering potent antibacterial activity.

Conclusion

In this study, HS-AgNPs were successfully produced using a cost-effective, biosafe, and environmentally friendly green synthesis method with *Hydrocotyle sibthorpioides* plant extract, as opposed to traditional methods, and integrated into PCL/PEO electrospun nanofibers for wound healing applications. Structural and morphological characterization results confirmed that HS-AgNPs are nano-sized, stable, and homogeneously distributed on the nanofiber surface. Thermal analyses revealed that the addition of HS-AgNPs increased the thermal stability of the hybrid fibers, while antimicrobial tests showed superior antibacterial activity, especially at high AgNP concentrations. Cytotoxicity analyses revealed that all nanofiber samples were compatible with fibroblast cells and did not produce any significant toxic effects. Hybrid nanofibers coated with biodegradable nanoparticles exhibit both improved thermal stability and strong antibacterial activity exceeding 99.99% against pathogens, supporting the potential of green technologies in wound healing processes. In conclusion, this study demonstrates that HS-AgNP-coated PCL/PEO nanofibers possess strong antibacterial activity, good thermal stability, and excellent cytocompatibility, making them promising candidates for wound dressing applications. From a translational perspective, these nanofibers may be particularly useful in the management of infected wounds, diabetic ulcers, or surgical site infections. However, further studies, such as in vivo wound healing models, long-term silver ion release kinetics, shelf-life stability under different storage conditions, and efficacy assessments against multidrug-resistant bacterial strains, are crucial for future prospects before transitioning to clinical application. The findings indicate that HS-AgNP-coated nanofibers are a multifunctional and promising wound dressing material with high antibacterial activity, stability, and biocompatibility, and constitute a strong candidate for biomedical applications.

Acknowledgements This study was conducted for research purposes within the scope of project number 1919B012316634 supported by The Scientific and Technological Research Council of Türkiye (TÜBİTAK) 2209-A University Students Research Projects Program. The authors sincerely thank Dr. Adem Yavaş for his expertise and contributions in conducting the cytotoxicity experiments, which were crucial to this study.

Author contributions Feride Demir: Writing – review & editing, Writing – original draft, Visualization, Validation, Resources, Project administration, Methodology, Investigation, Formal analysis, Data collection, Conceptualization. Ömer Kesmez: Validation, Resources, Project advisor, Methodology, Funding acquisition, Formal analysis, Data collection, Conceptualization, Writing – original draft, Writing – review & editing.

Funding Open access funding provided by the Scientific and Technological Research Council of Türkiye (TÜBİTAK).

Data availability Datasets used or evaluated in the study are available through the corresponding author upon reasonable request.

Declarations

Competing interests The authors declare no competing interests.

Open Access This article is licensed under a Creative Commons Attribution 4.0 International License, which permits use, sharing, adaptation, distribution and reproduction in any medium or format, as long as you give appropriate credit to the original author(s) and the source, provide a link to the Creative Commons licence, and indicate if changes were made. The images or other third party material in this article are included in the article's Creative Commons licence, unless indicated otherwise in a credit line to the material. If material is not included in the article's Creative Commons licence and your intended use is not permitted by statutory regulation or exceeds the permitted use, you will need to obtain permission directly from the copyright holder. To view a copy of this licence, visit http://creativecommons.org/licenses/by/4.0/.

References

1. Sun N, Zhu J, Li Y, Hu F, Dong J, Shen S, Xu X, Cao X, Zhou Z, Wong HM, Wu L, Li Q-L (2025) A multifunctional semi-interpenetrating polymer network hydrogel dressing for wound healing. Colloids Surf B 232:114616. https://doi.org/10.1016/j.colsurfb.2025.114616
2. Noor NM, Özgen S, Özbaş Z (2024) Development of thymol-loaded polymeric films designed as wound dressing materials: Physical, antioxidant, antibacterial, cytocompatibility, and wound healing properties. J Drug Deliv Sci Technol 97:105744. https://doi.org/10.1016/j.jddst.2024.105744
3. Anbumani A, Radhika S, Padma CM (2024) Synergistic effect of polyvinyl alcohol and *Datura stramonium*: Approach towards active wound dressing. J Ind Eng Chem 134:289–300. https://doi.org/10.1016/j.jiec.2023.12.059
4. Malik H, Amir F, Jahan Z, Liaqat U, Andleeb S, Bandyopadhyay S, Khan Niazi MB (2025) Study of shape of zinc oxide nanoparticles on the in-vitro and in-vivo performance of polymeric hydrogels for wound dressing. Int J Pharm 674:125482. https://doi.org/10.1016/j.ijpharm.2025.125482
5. Wang X, Li Q, Miao Y, Chen X, Zhang X, Shi J, Liu F, Wang X, Li Z, Yang Y, Zhang X, Wang J, Duan J (2023) A 0D-2D heterojunction bismuth molybdate-anchored multifunctional hydrogel for highly efficient eradication of drug-resistant bacteria. ACS Nano 17(16):15568–15589. https://doi.org/10.1021/acsnano.3c02304
6. Ding Y, Zhu Z, Zhang X, Wang J (2024) Novel functional dressing materials for intraoral wound care. Adv Healthc Mater 13(23):2400912. https://doi.org/10.1002/adhm.202400912
7. Brumberg V, Astrelina T, Malivanova T, Samoilov A, Angelis D, Gentile P, Toma L, Tanaka R (2021) Modern wound dressings: Hydrogel dressings. Biomedicines 9(9):1235. https://doi.org/10.3390/biomedicines9091235
8. Soylu Z, Oktay B, Erarslan A, Ahlatcıoğlu Özerol E (2025) Multifunctional polymeric wound dressings. Polym Bull 82(11):5325–5383. https://doi.org/10.1007/s00289-025-05753-z
9. Ho TTP, Tran HA, Doan VK, Maitz J, Li Z, Wise SG, Lim KS, Rnjak-Kovacina J (2024) Natural polymer-based materials for wound healing applications. Adv NanoBiomed Res 4(5):2300131. https://doi.org/10.1002/anbr.202300131

10. Gobi R, Ravichandiran P, Babu RS, Yoo DJ (2021) Biopolymer and synthetic polymer-based nanocomposites in wound dressing applications: A review. *Polymers, 13*(12), 1962. https://doi.org/10.3390/polym13121962
11. Lanno GM, Ramos C, Preem L, Putrins M, Laidmaë I, Tenson T, Kogermann K (2020) Antibacterial porous electrospun fibers as skin scaffolds for wound healing applications. ACS Omega 5(46):30011–30022. https://doi.org/10.1021/acsomega.0c04402
12. Lu X, Zhou L, Song W (2024) Recent progress of electrospun nanofiber dressing in the promotion of wound healing. Polymers 16(18):2596. https://doi.org/10.3390/polym16182596
13. Zulkifli MZA, Nordin D, Shaari N, Kamarudin SK (2023) Overview of electrospinning for tissue engineering applications. Polymers 15(11):2418. https://doi.org/10.3390/polym15112418
14. Yang J, Xu L (2023) Electrospun nanofiber membranes with various structures for wound dressing. Materials 16(17):6021. https://doi.org/10.3390/ma16176021
15. Devin PK, Farahpour MR, Tabatabaei ZG (2025) Multicomponent biopolymer hydrogels based on polycaprolactone with the combination of nano silver and linalool for the healing of infectious wounds. Int Immunopharmacol 148:114075. https://doi.org/10.1016/j.intimp.2025.114075
16. Ivanova AA, Syromotina DS, Shkarina SN, Shkarin R, Cecilia A, Weinhardt V, Baumbach T, Saveleva MS, Gorin DA, Douglas TEL, Parakhonskiy BV, Skirtach AG, Cools P, De Geyter N, Morent R, Oehr C, Surmeneva MA, Surmenev RA (2018) Effect of low-temperature plasma treatment of electrospun polycaprolactone fibrous scaffolds on calcium carbonate mineralisation. RSC Adv 8(68):39106–39114. https://doi.org/10.1039/c8ra07386d
17. Abbasi N, Soudi S, Hayati-Roodbari N, Dodel M, Soleimani M (2014) The effects of plasma treated electrospun nanofibrous poly(ε-caprolactone) scaffolds with different orientations on mouse embryonic stem cell proliferation. Cell J (Yakhteh) 16(3):245. https://www.ncbi.nlm.nih.gov/pmc/articles/PMC4204185/
18. Kim D, Choi H, Lee MJ, Cho WJ, Lee GW, Seo YK, Arai Y, Lee SH (2024) Oxygen plasma-modified polycaprolactone nanofiber membrane activates the biological function in cell adhesion, proliferation, and migration through the phosphorylation of FAK and ERK1/2, enhancing bone regeneration. Chem Eng J 499:156003. https://doi.org/10.1016/j.cej.2024.156003
19. Song Y, Li L, Zhao W, Qian Y, Dong L, Fang Y, Yang L, Fan Y (2021) Surface modification of electrospun fibers with mechano-growth factor for mitigating the foreign-body reaction. Bioactive Mater 6(9):2983–2998. https://doi.org/10.1016/J.BIOACTMAT.2021.02.020
20. Sun X, Ren H, Cui YC, Liu Q, Li J, Gao J (2025) Surface-induced self-assembly of peptides turns superhydrophobic surface of electrospun fibrous into superhydrophilic one. Colloids Surf B 245:114350. https://doi.org/10.1016/j.colsurfb.2024.114350
21. Ardeh DN, Nourbakhsh MS, Montazeri A, Rastegar H, Kari AY (2025) Fabrication and biological properties of electrospun chitosan/polyethylene oxide nanofibrous scaffolds loaded with the *Arctium lappa* L. extract. Int J Biol Macromol 308:142544. https://doi.org/10.1016/j.ijbiomac.2025.142544
22. Park SJ, Hwang T, Jo SH, Wooh S, Lee H, Jung Y, Yoo J (2025) Unveiling the diverse principles for developing sprayable hydrogels for biomedical applications. Biomacromolecules. https://doi.org/10.1021/acs.biomac.4c01312
23. Unnikrishnan U, Muthuswamy G, Kolanthai S, Megha E, Thomas M, Haris J, Gopinath M, Varghese G, R., Ayyasamy S (2024) Synthesis and analysis of multifunctional graphene oxide/Ag_2O-PVA/chitosan hybrid polymeric composite for wound healing applications. Int J Biol Macromol 277:134301. https://doi.org/10.1016/j.ijbiomac.2024.134301
24. Huang HC, Liaw CC, Zhang LJ, Ho HU, Kuo LMY, Shen YC, Kuo YH (2008) Triterpenoidal saponins from *Hydrocotyle sibthorpioides*. Phytochemistry 69(7):1597–1603. https://doi.org/10.1016/j.phytochem.2008.01.005
25. Lin X, Huang R, Zhang S, Wei L, Zhuo L, Wu X, Tang A, Huang Q (2013) Beneficial effects of asiaticoside on cognitive deficits in senescence-accelerated mice. Fitoterapia 87(1):69–77. https://doi.org/10.1016/j.fitote.2013.03.023
26. Arya AK, Durgapal M, Bachheti A, Deepti, Joshi KK, Gonfa YH, Bachheti RK, Husen A (2022) Ethnomedicinal use, phytochemistry, and other potential application of aquatic and semiaquatic medicinal plants. Evidence-Based Complement Altern Med 2022(1):4931556. https://doi.org/10.1155/2022/4931556
27. Lu J, Wang F (2024) Phytochemical properties and therapeutic potential of *Hydrocotyle vulgaris*: A systematic review. Med Plant Res. https://doi.org/10.5376/mpr.2024.14.0014

28. Li M, Li M, Wang L, Li M, Wei J (2023) Apiaceae medicinal plants: A review of traditional uses, phytochemistry, bolting and flowering, and controlling approaches. Preprints. https://doi.org/10.20944/preprints202212.0272.v2
29. Poonam, Kumar M (2020) Wetland plants: Recent advances in removal of pollutants from contaminated site. Contaminants Clean Technol 25–52. https://doi.org/10.1201/9780429275852-3
30. Yu F, Yu F, McGuire PM, Li R, Wang R (2007) Effects of *Hydrocotyle sibthorpioides* extract on transplanted tumors and immune function in mice. Phytomedicine 14(2–3):166–171. https://doi.org/10.1016/j.phymed.2006.03.010
31. Wu YH (2016) Naturally derived anti-hepatitis B virus agents and their mechanism of action. World J Gastroenterol 22(1):188. https://doi.org/10.3748/wjg.v22.i1.188
32. Patel K, Mishra R, Kumar Patel D (2016) A review on phytopharmaceutical importance of asiaticoside. Medicine 4(12):1000–1007. https://doi.org/10.12980/jclm.4.2016J6-161
33. Talukdar S, Gupta A (2020) Ethnomedicinal knowledge of the Garo community of two villages in western Assam, India. J Herb Med 20:100229. https://doi.org/10.1016/j.hermed.2018.08.004
34. Xia J, Inagaki Y, Song P, Sawakami T, Kokudo N, Hasegawa K, Sakamoto Y, Tang W (2016) Advance in studies on traditional Chinese medicines to treat infection with the hepatitis B virus and hepatitis C virus. Biosci Trends 10(5):327–336. https://doi.org/10.5582/bst.2016.01110
35. Zhang Q, Feng Y, Kennedy D (2016) Multidrug-resistant cancer cells and cancer stem cells hijack cellular systems to circumvent systemic therapies: Can natural products reverse this? Cell Mol Life Sci 74(5):777–801. https://doi.org/10.1007/s00018-016-2362-3
36. Hazarika I, Mukundan GK, Sundari PS, Laloo D (2021) Journey of *Hydrocotyle sibthorpioides* Lam.: From traditional utilization to modern therapeutics—A review. Phytother Res 35(4):1847–1871. https://doi.org/10.1002/ptr.6924
37. Hazarika I, Geetha KM, Sundari PS, Madhu D (2019) Acute oral toxicity evaluation of extracts of *Hydrocotyle sibthorpioides* in Wistar albino rats as per OECD 425 TG. Toxicol Rep 6:321–328. https://doi.org/10.1016/j.toxrep.2019.04.001
38. Ibrahim AM, Musthaque KM, Nandhagopal S (2026) Green synthesis and evaluation of lithium oxide nanoparticles for antimicrobial and photocatalytic applications. J Appl Spectrosc 92:1398–1407. https://doi.org/10.1007/s10812-026-02051-y
39. Tarannum N, Divya, Gautam YK (2019) Facile green synthesis and applications of silver nanoparticles: A state-of-the-art review. RSC Adv 9(60):34926–34948. https://doi.org/10.1039/c9ra04164h
40. Menéndez Miranda M, Liu W, Godinez-Leon JA, Amanova A, Houel-Renault L, Lampre I, Remita H, Gref R (2023) Colloidal silver nanoparticles obtained via radiolysis: Synthesis optimization and antibacterial properties. Pharmaceutics 15(7):1787. https://doi.org/10.3390/pharmaceutics15071787
41. Singaravelan R, Bangaru S, Alwar S (2015) Electrochemical synthesis, characterisation and phytogenic properties of silver nanoparticles. Appl Nanosci 5(8):983–991. https://doi.org/10.1007/s13204-014-0396-0
42. Singh R, Shedbalkar UU, Wadhwani SA, Chopade BA (2015) Bacteriagenic silver nanoparticles: Synthesis, mechanism, and applications. Appl Microbiol Biotechnol 99(11):4579–4593. https://doi.org/10.1007/s00253-015-6622-1
43. Imchen L, Manisekaran R, Jamir I, Rathore HS, Senthilvelan T (2025) A review on plant-mediated synthesis of AgNPs and their formulations for wound healing application. Mol Biol Rep 52(1):1–17. https://doi.org/10.1007/s11033-025-10512-4
44. Saber MM, Mirtajani SB, Karimzadeh K (2018) Green synthesis of silver nanoparticles using *Trapa natans* extract and their anticancer activity against A431 human skin cancer cells. J Drug Deliv Sci Technol 47:375–379. https://doi.org/10.1016/j.jddst.2018.08.004
45. Vanlalveni C, Lallianrawna S, Biswas A, Selvaraj M, Changmai B, Rokhum SL (2021) Green synthesis of silver nanoparticles using plant extracts and their antimicrobial activities: A review of recent literature. RSC Adv 11(5):2804–2837. https://doi.org/10.1039/d0ra09941d
46. Garg M, Devi B, Devi R (2017) In vitro antibacterial activity of biosynthesized silver nanoparticles from ethyl acetate extract of *Hydrocotyle sibthorpioides* against multi-drug-resistant microbes. Asian J Pharm Clin Res 10(6):263–266. https://doi.org/10.22159/ajpcr.2017.v10i6.17976
47. Bashir N, Afzaal M, Khan AL, Nawaz R, Irfan A, Almaary KS, Dabiellil F, Bourhia M, Ahmed Z (2025) Green-synthesized silver nanoparticle-enhanced nanofiltration mixed matrix membranes for high-performance water purification. Sci Rep 15(1):1–16. https://doi.org/10.1038/s41598-024-83801-w

48. Widatalla HA, Yassin LF, Alrasheid AA, Rahman Ahmed SA, Widdatallah MO, Eltilib SH, Mohamed AA (2022) Green synthesis of silver nanoparticles using green tea leaf extract, characterization and evaluation of antimicrobial activity. Nanoscale Adv 4(3):911–915. https://doi.org/10.1039/D1NA00509J
49. Kesmez Ö (2020) Preparation of anti-bacterial biocomposite nanofibers fabricated by electrospinning method. J Turkish Chem Soc Sect A: Chem 7(1):125–142. https://doi.org/10.18596/JOTCSA.590621
50. Nazemoroaia M, Bagheri F, Mirahmadi-Zare SZ, Eslami-Kaliji F, Derakhshan A (2025) Asymmetric natural wound dressing based on porous chitosan-alginate hydrogel/electrospun PCL-silk sericin loaded by 10-HDA for skin wound healing: In vitro and in vivo studies. Int J Pharm 668:124976. https://doi.org/10.1016/j.ijpharm.2024.124976
51. Eghbalifam N, Shojaosadati SA, Hashemi-Najafabadi S (2023) Role of bioactive magnetic nanoparticles in the prevention of wound pathogenic biofilm formation using smart nanocomposites. BMC Chem 17(1):1–21. https://doi.org/10.1186/s13065-023-00965-8
52. Caponio F, Alloggio V, Gomes T (1999) Phenolic compounds of virgin olive oil: influence of paste preparation techniques. Food Chem 64(2):203–209. https://doi.org/10.1016/S0308-8146(98)00146-0
53. Ahmad W, Jaiswal KK, Soni S (2020) Green synthesis of titanium dioxide (TiO_2) nanoparticles by using *Mentha arvensis* leaves extract and its antimicrobial properties. Inorg Nano-Metal Chem 50(10):1032–1038. https://doi.org/10.1080/24701556.2020.1732419
54. Hezari S, Olad A, Dilmaghani A (2022) Modified gelatin/iron-based metal-organic framework nanocomposite hydrogel as wound dressing: Synthesis, antibacterial activity, and *Camellia sinensis* release. Int J Biol Macromol 218:488–505. https://doi.org/10.1016/j.ijbiomac.2022.07.150
55. Yadav V, Galatage ST, Manjappa AS, Salawi A, Peram MR, Nadaf SJ, Harale SS (2024) Green synthesis of silver nanoparticles from *Clematis gouriana* leaf extract: Physicochemical characterization and antibacterial activity determination for treatment of blood stream infections. Microbe 5:100197. https://doi.org/10.1016/J.MICROB.2024.100197
56. Ganachari SV, Bhat R, Deshpande R, Venkataraman A (2012) Extracellular biosynthesis of silver nanoparticles using fungi *Penicillium diversum* and their antimicrobial activity studies. BioNanoScience 2(4):316–321. https://doi.org/10.1007/S12668-012-0046-5/TABLES/1
57. Rajput SK, Banerjee S, Sharma V, Ali SW, Singh MK, Shakyawar DB (2025) A facile and greener approach for synthesis of lignin capped-silver nanoparticles (LS-AgNPs) and assessment of their antibacterial and antioxidant properties. J Mol Struct 1322:140515. https://doi.org/10.1016/j.molstruc.2024.140515
58. Sodha KH, Jadav JK, Gajera HP, Rathod KJ (2015) Characterization of silver nanoparticles synthesized by different chemical reduction methods. Int J Pharma Bio Sci 6(4):199–208. https://www.researchgate.net/publication/320183631
59. Raja K, Saravanakumar A, Vijayakumar R (2012) Efficient synthesis of silver nanoparticles from *Prosopis juliflora* leaf extract and its antimicrobial activity using sewage. Spectrochimica Acta - Part A: Mol Biomol Spectrosc 97:490–494. https://doi.org/10.1016/j.saa.2012.06.038
60. Hussain Z, Raza MA, Jahangeer M, Sarwar A, Nadeem AA, Naz S, Aziz T, Alharbi M, Alshammari A, Alasmari AF (2023) Green synthesis of silver nanoparticles prepared by leaves extract of *Trigonila foenum-graecum* and its antibacterial potential against *Escherichia coli* and *Pseudomonas aeruginosa*. *Biomass Conversion and Biorefinery.* https://doi.org/10.1007/s13399-023-04852-z
61. Alomar TS, Almasoud N, Awad MA, Alomar RS, Merghani NM, El-Zaidy M, Bhattarai A (2024) Designing green synthesis-based silver nanoparticles for antimicrobial theranostics and cancer invasion prevention. Int J Nanomed 19:4451–4464. https://doi.org/10.2147/IJN.S440847
62. Abbigeri MB, Thokchom B, Singh SR, Bhavi SM, Harini BP, Yarajarla RB (2025) Antioxidant and anti-diabetic potential of the green synthesized silver nanoparticles using *Martynia annua* L. root extract. Nano TransMed 4:100070. https://doi.org/10.1016/J.NTM.2025.100070
63. Al-Khayri JM, Sahana GR, Nagella P, Joseph BV, Alessa FM, Al-Mssallem MQ (2022) Flavonoids as potential anti-inflammatory molecules: A review. Molecules 27(9):2901. https://doi.org/10.3390/molecules27092901
64. Kumari S, Elancheran R, Kotoky J, Devi R (2016) Rapid screening and identification of phenolic antioxidants in *Hydrocotyle sibthorpioides* Lam. by UPLC–ESI-MS/MS. Food Chemistry, 203, 521–529. https://doi.org/10.1016/j.foodchem.2016.02.101
65. Criollo-Mendoza MS, Contreras-Angulo LA, Leyva-López N, Gutiérrez-Grijalva EP, Jiménez-Ortega LA, Heredia JB (2023) Wound Healing Properties of Natural Products. Mech Action Molecules 28(2):598. https://doi.org/10.3390/molecules28020598

66. Shin HY, Kim YS, Ha EJ, Koo JP, Jeong WB, Joung MY, Shin KS, Yu KW (2024) Anti-inflammatory action and associated intracellular signaling of *Centella asiatica* extract on lipopolysaccharide-stimulated RAW 264.7 macrophage. Food Bioscience 61:104614. https://doi.org/10.1016/j.fbio.2024.104614
67. Usharani S, Panneerselvam R, Flora PJ (2023) Green synthesis of silver nanoparticles using *Centella asiatica* and evaluation of its anticancer activity. Int J Zoological Investigations 9(1):749–761. https://doi.org/10.33745/ijzi.2023.v09i01.084
68. Shah SA, Gul A, Shah GM, Shah M, Iqbal S, Mahmood S (2024) Phytochemical analyses and bioactivities of various solvent extracts of Onychium japonicum (Thunb.) Kunze and its greenly synthesized silver nanoparticles. Inorg Chem Commun 167:112782. https://doi.org/10.1016/j.inoche.2024.112782
69. Yao Y, Wei H, Wang J, Lu H, Leng J, Hui D (2015) Fabrication of hybrid membrane of electrospun polycaprolactone and polyethylene oxide with shape memory property. Compos Part B: Eng 83:264–269. https://doi.org/10.1016/j.compositesb.2015.08.060
70. Wardhani RAK, Asri L, Nasir M, Purwasasmita BS (2019) Preparation of chitosan-polyethylene oxide-*Colocasia esculenta* flour nanofibers using electrospinning method. J Mech Eng Sci Technol 3(1):1–7. https://doi.org/10.17977/um016v3i12019p001
71. Afshar A, Majd H, Harker A, Edirisinghe M (2024) Tailored binary polymer system PCL-PEO for advanced biomedical applications: Optimization, characterization and *in vitro* analysis. J Drug Deliv Sci Technol 95:105582. https://doi.org/10.1016/j.jddst.2024.105582
72. Gün Gök Z, Yiğitoğlu M, Vargel İ, Şahin Y, Alçığır ME (2021) Synthesis, characterization and wound healing ability of PET-based nanofiber dressing material coated with silk sericin capped silver nanoparticles. Mater Chem Phys 259:124043. https://doi.org/10.1016/j.matchemphys.2020.124043
73. Phan DN, Dorjjugder N, Saito Y, Taguchi G, Ullah A, Kharaghani D, Kim IS (2020) The synthesis of silver-nanoparticle-anchored electrospun polyacrylonitrile nanofibers and a comparison with as-spun silver/polyacrylonitrile nanocomposite membranes upon antibacterial activity. Polym Bull 77(8):4197–4212. https://doi.org/10.1007/s00289-019-02969-8
74. Lin MC, Lin JH, Huang CY, Chen YS (2020) Tissue engineering stent model with long fiber-reinforced thermoplastic technique. J Mater Science: Mater Med 31(11):1–12. https://doi.org/10.1007/s10856-020-06411-8
75. ASTM International (n.d.) Test method for water absorption of plastics (ASTM D570). ASTM Int. https://doi.org/10.1520/D0570
76. Rodriguez C, Padilla V, Lozano K, McDonald A, Materon L, Chapa A, Ahmad F, De Leo CT, Gilkerson R (2021) Fabrication of Forcespinning® nanofibers incorporating nopal extract. Polym Int 70(5):679–686. https://doi.org/10.1002/pi.6163
77. ASTM International (2002) ASTM D882-02: Standard test method for tensile properties of thin plastic sheeting, vol 08.01, p. 9. Available online: https://doi.org/10.1520/D0882-02
78. Niknejad E, Jafari R, Valipour Motlagh N (2025) Mechanical properties of biodegradable fibers and fibrous mats: A comprehensive review. Molecules 30(15):3276. https://doi.org/10.3390/molecules30153276
79. Ribeiro ARM, Teixeira MO, Ribeiro L, Tavares TD, Miranda CS, Costa AF, Ribeiro A, Silva MM, Silva C, Felgueiras HP (2024) Sodium alginate-based multifunctional sandwich-like system for treating wound infections. Biomaterials Adv 213931. https://doi.org/10.1016/j.bioadv.2024.213931
80. Mikhailova EO (2025) Green Silver Nanoparticles: An Antibacterial Mechanism. Antibiotics 14(1):5. https://doi.org/10.3390/antibiotics14010005
81. Gwada CA, Ndivhuwo PS, Matshetshe K, Aradi E, Mdluli P, Moloto N, Otieno F, Airo M (2025) Phytochemical-assisted synthesis, optimization, and characterization of silver nanoparticles for antimicrobial activity. RSC Adv 15:14170–14181. https://doi.org/10.1039/D4RA08900F
82. Krishnan PD, Banas D, Durai RD, Kabanov D, Hosnedlova B, Kepinska M, Fernandez C, Ruttkay-Nedecky B, Nguyen HV, Farid A, Sochor J, Narayanan VHB, Kizek R (2020) Silver nanomaterials for wound dressing applications. Pharmaceutics 12(9):821. https://doi.org/10.3390/pharmaceutics12090821
83. Eker F, Akdaşçi E, Duman H, Bechelany M, Karav S (2025) Green synthesis of silver nanoparticles using plant extracts: A comprehensive review of physicochemical properties and multifunctional applications. Int J Mol Sci 26(13):6222. https://doi.org/10.3390/ijms26136222
84. ISO (2009) *Biological evaluation of medical devices - Part 5: Tests for in vitro cytotoxicity (ISO 10993-5:2009).* International Organization for Standardization. https://mdcpp.com/doc/standard/ENISO10993-5-2009.pdf

85. Hussain Z, Raza MA, Jahangeer M et al (2024) Green synthesis of silver nanoparticles prepared by leaves extract of *Trigonella foenum-graecum* and its antibacterial potential against *Escherichia coli* and *Pseudomonas aeruginosa*. *Biomass Conversion and Biorefinery*, 14, 31431–31438. https://doi.org/10.1007/s13399-023-04852-z
86. Ielo I, Bauso LV, Laezza A, Campione P, Fabiano L, Pastorello M, Marino A, Laurita A, Pepe A, Bochicchio B et al (2025) In Vitro Assessment of Electrospun PVP+AgNPs Scaffolds for Bioactive Medical Use. Int J Mol Sci 26:9114. https://doi.org/10.3390/ijms26189114

Publisher's note Springer Nature remains neutral with regard to jurisdictional claims in published maps and institutional affiliations.

Authors and Affiliations

Feride Demïr[1] · Ömer Kesmez[1]

✉ Ömer Kesmez
omerkesmez@akdeniz.edu.tr

Feride Demir
feride.demirc@gmail.com

[1] Department of Chemistry, Faculty of Science, Akdeniz University, Antalya 07070, Türkiye, Turkey